EUDET-Memo-2008-37

Experimental validation of optical simulations
for microstrip detectors[*]

M. Fernández, J. González, R. Jaramillo,

A. López, C.M. Rivero, D. Moya, A. Ruiz, I. Vila

Instituto de Física de Cantabria, Universidad de Cantabria and CSIC, Santander (Spain)

D. Bassignana, E. Cabruja, M. Lozano, G. Pellegrini

Centro Nacional de Microelectrónica, IMB-CNM/CSIC, Barcelona, (Spain)

December 17, 2008

Abstract

We present the comparison of simulated and measured optical functions (reflectance and transmittance) of samples of materials employed in the fabrication of silicon microstrip detectors. Using our simulation we are able to extract the refraction indexes of these samples in the near infrared wavelength range. We then use this information as input of a full optical simulation of microstrips detectors, taking into account diffraction effects in the strips. Both simulations are validated against measurements. First measurements of new sensors for the alignment system of the SiTRA prototype are also presented in this work.

1

1 Introduction

For the particular case of tracking detectors, a very elegant alignment method has been recently proposed and implemented [1] at the Alpha Magnetic Spectrometer (AMS) [2] and subsequently adopted [3] by the tracking system of the Compact Muon Solenoid [4]. In a nutshell, consecutive layers of silicon sensors are traversed by IR laser beams which play the role of infinite momentum tracks (not bent by the magnetic field). Then, the same sophisticated alignment algorithms as employed for track alignment with real particles can be applied to achieve few microns relative alignment between modules. Furthermore, since IR light produces a measurable signal in the silicon bulk, there is no need for any extra readout electronics. And all these advantages come to a minimum cost: a small circular window (few mm diameter) on the aluminum back-metalization must be open to allow the IR beam to pass through.

In a previous work [5] we identified the key parameters that determine the overall transmittance of a microstrip detector. We found that the pitch to strip ratio (i.e., the fraction of the sensor covered by Aluminum) determines the percentage transmitted through the detector. The smaller the strip width, the more light is transmitted. A good balance between maximum transmittance and finite strip width was set to 10% of the pitch. Therefore changes in the layout rather than changes in the detector thickness seem to boost the transmittance reach of microstrip detectors. Further tuning of layer thickness will normally contribute to $\approx 5\%$ over the layout optimized value.

This paper is the continuation of that previous work [5]. We present now the validation of the simulation of continuous optical media, comparing the calculated Transmittance (T) and Reflectance (R) with that of real material samples. These measurements were obtained with a spectrophotometer presented in next section. A comprehensive study of Silicon optical properties and comparison with other published results will be shown in section 3. The validation of the structured multilayer grating simulation will be shown in section 4. The last section of this paper will show optical measurements of new alignment modified Hamamatsu silicon microstrips [6], produced within the SiLC collaboration and the validation of laser reconstruction using these same sensors.

2 Spectroscopic measurements

A spectrometer measures the intensity of light as a function of wavelength, within a wavelength range with certain resolution. One can roughly speak of single beam or double beam spectrometers. The latter compares the intensity of light in 2 paths, one of them having the sample to be measured. In single beam spectrometers, the ratio of intensity with and without sample is compared. Double beam spectrometers are more complicated and expensive than single beam, but are normally more precise and accurate.

Within single beam spectrometers, the most common are dispersive type spectrometers and Fourier Transform (FT) spectrometers. In the first class, the individual frequencies are separated by the use of a prism or grating. A detector measures the amount of energy

at each frequency that passes through the sample, thus dividing the total intensity in its spectral components. FT spectrometers have a beamsplitter, one fixed mirror and one movable mirror that make up an interferometer. All frequencies are measured at the same time. A Fourier transformation analysis allows to decode the information of each individual wavelength. FT are faster than dispersive apparatus. On the other hand, dispersive spectrometers are more robust (no movable parts), compact and provide good resolution by averaging several samples of spectra.

The most important parameters of a spectrometer for our application were the wavelength range and the instrument spectral resolution. This last parameter is the key to separate contiguous interference peaks. Driven by these constraints we finally chose a custom made dispersive system from Control Development with 1.2 nm spectral resolution over the range 955-1155 nm [7]. A picture of the spectrophotometer is shown in Figure 1, under a configuration of T measurement. The light from the halogen lamp [8] is conducted with optical fibers [9] and collimated on the sample placed on a height adjustable RT table [10]. The transmitted light is collected by the return (or measurement) fiber and analyzed by the spectrometer unit. The DAQ is done with a standard PC connected to the spectrometer using a USB cable.

The effect of the spectral resolution in the spectrometer is show in Figs 2 and 3. The resolving power of the spectrometer mixes up intensity peaks closer than 1.2 nm. Mathematically this can be expressed as a convolution of the ideal spectrum with a gaussian as explained in [11].

3 Validation of continuous optical media simulation

Calculation of the optical functions of a multilayer is well understood and has been extensively treated (see for instance ref. [12]). Qualitatively, when the media are perfectly planoparallel, reflections in the interfaces are specular. If a medium is absorbing, then the intensity of the transmitted wave will be damped following Lambert's exponential law. In any case, a coherent sum of amplitudes will account for the transmitted and reflected intensity. If any interface between two media is rough, then the reflectance will have two components: specular and diffuse. The loss of specular reflectance due to roughness can be accounted multiplying the Fresnel coefficients of the ideal layer by an exponential factor, see for instance [13].

Two types of problems are normally faced in spectrometry. In the direct problem, the optical functions T and R of the multilayer are calculated from the refraction indexes and thicknesses of the materials. In the inverse problem, measured optical functions are used to extract the refraction indexes and thickness of the layers. As already explained in our previous paper [5], we have chosen a χ^2 minimization technique to solve the inverse problem. In this method, measured T_{meas}, R_{meas} are compared at each wavelength with calculated values, and the difference is minimized:

$$\chi^2 = \sum_\lambda \left(\frac{T_{calc}(\lambda, n(\lambda), k(\lambda), d) - T_{meas}(\lambda)}{\sigma_T(\lambda)} \right)^2 + \left(\frac{R_{calc}(\lambda, n(\lambda), k(\lambda), d) - R_{meas}(\lambda)}{\sigma_R(\lambda)} \right)^2 \quad (1)$$
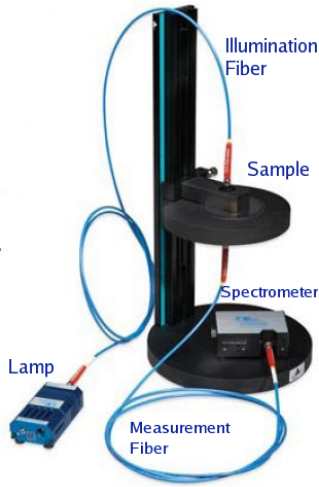
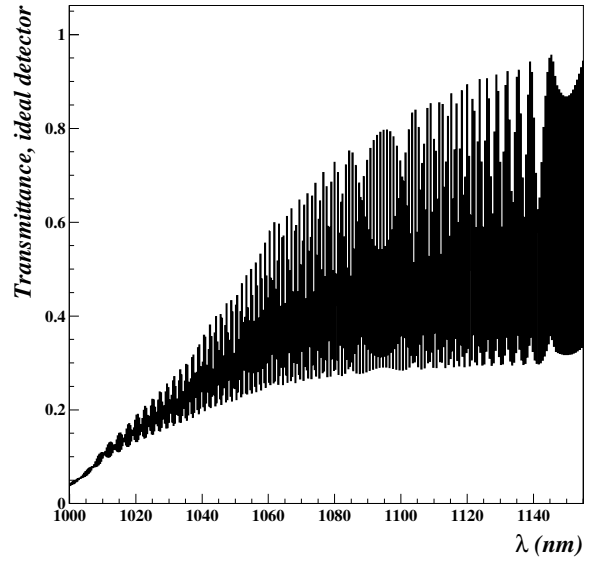Figure 1: *Spectrophotometer showing the configuration for a transmittance measurement*

Figure 2: *Simulated transmittance spectrum of a 295 µm thick Si wafer assuming a perfect spectrophotometer.*

with $\sigma_{T,R}$ the measurement error of the spectrometer. As this formula displays, T and R are functions of the wavelength, of the refraction index of the material and of its thickness. In turn, the real and imaginary part of the refraction index (n and k) are also functions of the wavelength.

To validate our implementation of the simulation and measurement procedure (using an inverse technique) we have successfully reproduced the measured reflectance of a commercially available reference wafer [14]. The wafer has 5 bands of SiO_2 on a thick Si substrate. While the front side of the wafer is polished, the backside silicon surface is rough. The thickness of SiO_2 is measured by the vendor at specific positions and range from 0-500 nm. This calibration is done using an ellipsometer with an accuracy of order $\sim O(1/10)$ nm. The refraction index of SiO2 is quoted as well by the manufacturer but only for $\lambda =$632.8 nm. Its value is approximately 5% smaller than standard tabulated silicon dioxide. Measuring the first band (uncoated Si) we obtained a wafer thickness of 530 μm with a back roughness of 120 nm. We also found that the tabulated refraction index of Si was suitable to describe the measured reflectance spectrum. Using these 2 inputs, the thickness of a band of SiO_2 was accurately calculated with an error lower than 2 nm. Fig. 4 shows the measured reflectance with errors (black graph) and the fitted
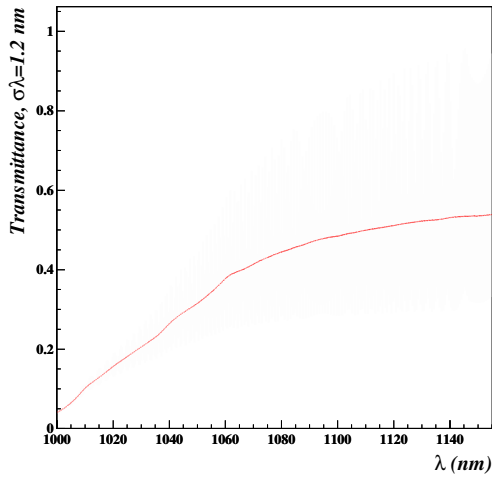
Figure 3: *Simulated transmittance spectrum of the same Si slab as in Fig. 2 assuming a spectrophotometer resolution of 1.2 nm*
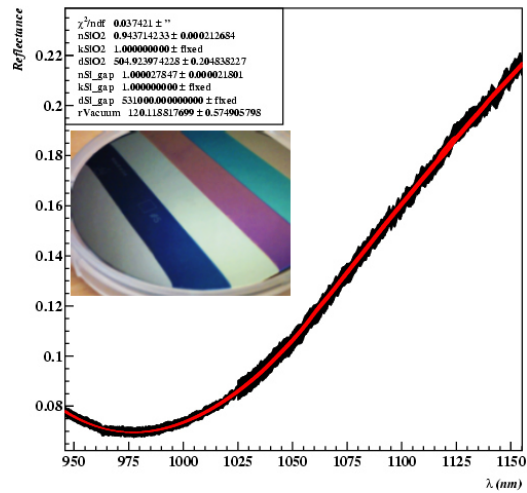

Figure 4: *Calculated (red line) and measured (black trace) reflectance of SiO_2 on Si. Inlaid picture shows the calibrated wafer where the different bands (different thickness) of SiO_2 are seen.*

reflectance (continuous red line) with the associated fit superimposed of a calibrated 502.64 nm SiO_2 band. A picture of the wafer is shown inlaid in the figure.

3.1 Optical characterization of Si in the NIR and comparison with published data

We have carried out an indepth characterization of our Si wafers, due to the importance of this material in the design of microstrip detectors. Our Si samples are double sided polished wafers, produced by TopSiL [15]. The thickness of several of those wafers was measured with a ≈1 μm resolution contact micrometer. The average thickness (randomly sampled) was 295.2 ± 0.8 μm. This value matches the (wide) thickness tolerance quoted by the foundry (± 15 μm).

Transmittance and reflectance of an unprocessed wafer were measured several times in different spots for both sides of the wafer. A repeatability of order 1% was found. This value falls within the repeatability of the spectrometer measurement.

3.1.1 Analytical expressions for the refraction index for short wavelengths ($\lambda < 1$ μm)

Prior to the combined fit of T and R, we obtained valuable information from a simple analysis of the low end λ spectra. To the best of our knowledge, this is a novel analysis. Photons with wavelengths below 1 μm in a thick slab of Si cannot reach the second surface of the wafer. This can be experimentally crosschecked in a reflectance measurement using a mirror on top of the Si wafer and illuminating the Si wafer from below. When the photons reach the second surface, the measured reflectance must be higher than that of the raw wafer, due to the presence of the mirror. This fact is shown in Fig. 5. The bottom spectrum shows the measured reflectance of a 295 μm thick wafer. The top plot shows the increased reflectance due to the mirror. As seen in this figure, both measurements coincide for $\lambda < 980$ nm. In this wavelength range ($\lambda < 980$ nm) the reflectance of the wafer must be similar to the reflectance of a single Si interface, since photons do not reach the second interface. From the formula of reflectance of a single interface on air:

$$R \quad = \quad \frac{(n-1)^2 + k^2}{(n+1)^2 + k^2} \approx \frac{(n-1)^2}{(n+1)^2} \tag{2}$$

with n the real part of the refraction index and k the extinction index of Si. The last approximation holds due to the different magnitude of both indexes (n$\approx$ 3.5,k$\approx$ 10^{-3} near λ=1 μm). So, inverting eq. (2):

$$n \quad = \quad \frac{1 + \sqrt{R}}{1 - \sqrt{R}} \tag{3}$$

Therefore one can compute n using last equation. Figure 6 shows the calculated refraction index values with the errors propagated from eq. 3.

Valuable information on the absorption coefficient of Si ($\lambda < 1$ μm) can be extracted from transmittance measurements. Indeed, we may abstract the first transmitted beam through the Si slab. Fig. 7 shows the incident beam arriving to a slab of thickness d. At this interface, a fraction R will be reflected (according to eq. 2) and another T_{12} transmitted. From the transmitted intensity, only a fraction $e^{-\alpha d}$ will reach the second surface (due to damping, α is the absorption coefficient) from which only T_{21} will exit. Since $T_{12} = T_{21}$ (see [12]), the 1st beam transmitted intensity will be:

$$T \quad = T_{12} \times T_{21} \times e^{-\alpha d} \quad = \left(\frac{4n}{(n+1)^2}\right)^2 e^{-\frac{4\pi}{\lambda} kd} \tag{4}$$

Using last expression to fit $T(\lambda < 1$ μm) as shown in Fig. 8 it is clear that only the product kd can be estimated. Now, making use of equation 3 we can also write eq. 4 as:

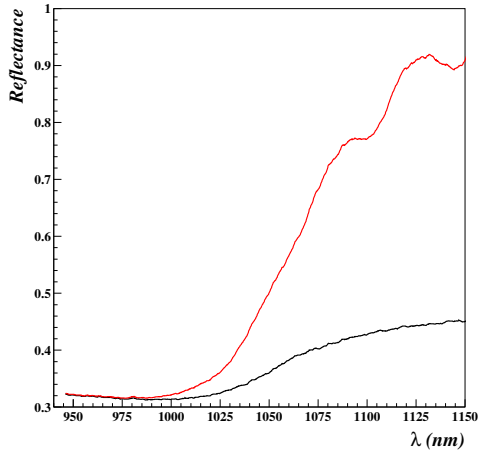Figure 5: *Reflectance of a 295 µm thick Si wafer (bottom curve). The top curve shows the measured reflectance when a mirror is placed on top of the second wafer interface.*

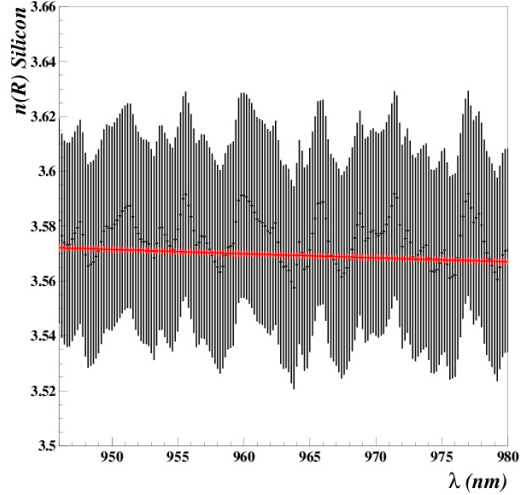Figure 6: *Analytical calculation of the real part of the refraction index, with errors.*

$$kd \quad = \quad \frac{\lambda}{4\pi} \log \frac{(1-R)^2}{T} \tag{5}$$

Both equations (3) and (5) can be used in the solution of the inverse problem by the χ^2 minimization technique. These equations plus the measured thickness will be used as constraints for n and k in the global fit of T and R ($\lambda \in [946, 1155]$).

3.2 Silicon refraction index in the near infrared

A comprehensive study of the optical properties of Si is found in former studies, mostly led by research on Si solar cells. In particular, Keevers and Green [16] offer high resolution measurements of the absorption coefficient α as a function of wavelength. This coefficient relates to the extinction coefficient by $\alpha = 4\pi k/\lambda$.

An analytical parametrization of the extinction coefficient is given by Geist in ref. [17]. This function depends on 15 parameters. Fortunately, some of these parameters could be fixed within our wavelength range of interest. We also fixed those parameters that were not free but had strong correlations with others in the parametrization. Finally we could reduce the number of parameters from 15 to 2 within the region $\lambda \in [1000, 1127]$ nm.
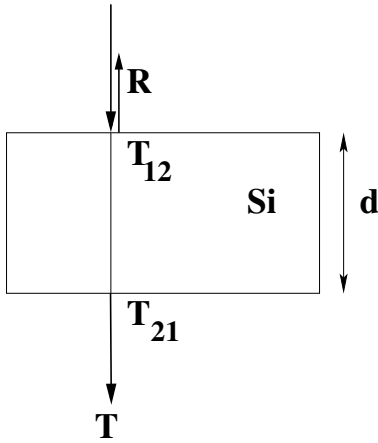
Figure 7: *Sketch of the trajectory of the 1ˢᵗ transmitted beam in the Si wafer. R stands for the reflectance of a single interface.*
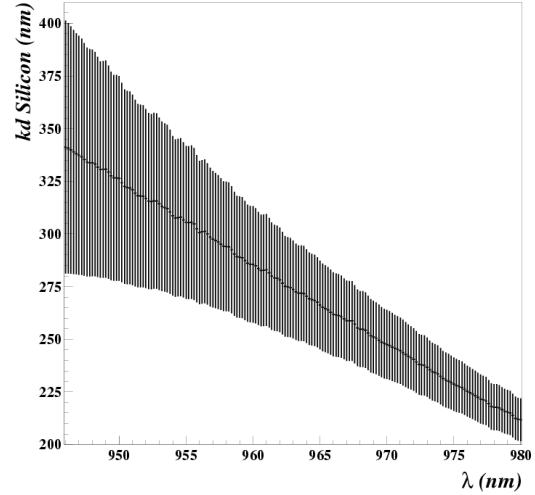

Figure 8: *Product kd calculated analytically from eq. 5. Error bars obtained from standard error propagation.*

For the real part of the refraction index, tabulated data and analytical forms are given in the same ref. [17]. However in a slightly former work [18] Keevers and Green override the accuracy of all other data up to now and provide as well a simpler analytical parametrization. According to this analytical form, we can use a single parameter model to describe n. As a comparison of the accuracy of the different sources, tabulated data for Geist (rounded markers), measurements from Keevers and Green (square markers) and their parametrization (continuous line) are shown in Fig. 9.a) for n.

Figure 9.b) shows a simultaneous fit of T and R for the unprocessed Silicon reference wafer from TopSiL, using the parameterizations for (n,k) cited above plus constraints. Measured data are displayed with their experimental error. Fig. 9.c) shows the real part of the refraction index obtained from the fit, as a function of the wavelength. For $\lambda < 980$ nm we have superimposed the analytically calculated index according to eq. (3). The continuous line is our fit and the evenly spaced points with errors are the tabulated data from [17] shown as reference.

4 Validation of structured multilayer grating simulation

A simulation of a microstrip detector must take into account the periodic segmentation of the microstrips. Whenever the obstacles to the incoming beam are comparable to the wavelength of light, diffraction occurs. The incoming beam breaks into a bunch of diffracted beams, each of them propagating under different angles. All these beams
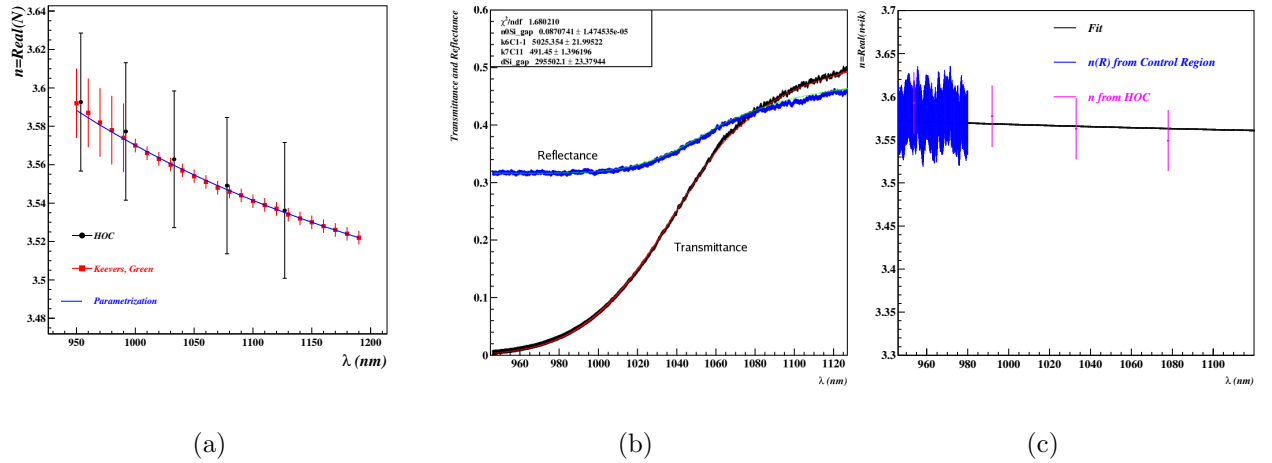
(a) (b) (c)

Figure 9: a) Comparison of two tabulated sets of refraction indexes for Si. Continuous line is the parametrization from reference [18]. b) Simultaneous fit of T and R for a Si slab using parameterizations for both components of the refraction index. c) Real part of the refraction index obtained from simultaneous fit of TR. The graph shown ($\lambda < 980$ nm) is obtained from eq. (3). Circular markers with error bars are tabulated Si data from ref. [17]

will suffer multiple reflections and will interfere. As we showed in ref. [5], the resulting transmitted or reflected intensity does not coincide with the calculation of perfect planoparallel layers, since that simulation does not take into account diffraction effects. The best way to account for the diffraction effects is solving Maxwell equations rigorously. The implementation of the solution of Maxwell equations for gratings benefit from the periodicity of the strips to express the electromagnetic fields as Fourier expansions in terms of space-harmonic fields . Though the solution is exact, the Fourier expansion must be truncated for calculation purposes, so the accuracy at the end will depend on the number of diffraction orders retained. We have chosen a method called Rigorous Coupled Wave Analysis (RCWA) to calculate the diffracted reflected and transmitted intensities. Full detailed explanation of the RCWA method can be found in ref. [19]. An open implementation of this method (RODIS software [20]) is available from the Photonics Research Group of U. Ghent.

4.1 Comparison to published results

First of all, we have compared the results of the simulation package against other published work. For instance, Fig. 10 shows the calculated 0 order transmitted diffraction efficiency (transmittance of the central diffracted beam), for TE and TM polarizations [21]. The agreement between the calculated efficiency (markers) and our simulation (contin-
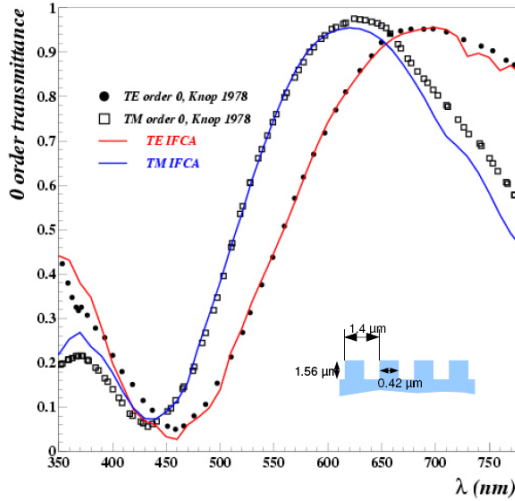
Figure 10: *Simulated TE (circular markers) and TM (squares) 0 order transmittance from ref. [21] compared to RODIS calculations (lines)*
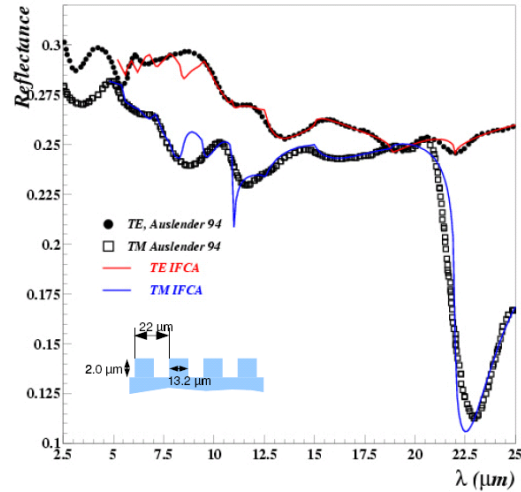
Figure 11: *TE (circles) and TM(squares) calculated reflectance [22] compared to RODIS calculations (continuous line).*

uous line) is quite good. Figure 11 shows a comparison of the global reflectance (all diffraction orders summed) with the calculated in ref [22]. Markers correspond to published calculations, and the continuous lines are our calculations using RODIS. In both figures, the simulated grating is also displayed inlaid in the figure. From these 2 comparisons we conclude that our simulated results are very similar to other calculations.

4.2 Measurements on real diffraction gratings

To test the predictions of this method on a real wafer, we have produced, within the facilities of CNM-IMB (GICSERV program) [23], a simple wafer containing a known structure of strips on Si. A picture of the wafer is shown in Fig. 12.a). A sketch of the layer structure is shown in Figure 12.b). This structure, though not a full functional sensor, contains the basic elements needed to study the transmitted and reflected diffraction efficiencies on a real sample. Figure 12.c) shows the calculated transmittance and reflectance for one of the individual sensors in the wafer. We have kept 40 diffraction orders in this calculation. Though the transmittance is remarkably well explained, the calculated reflectance is still higher than the measured value. We are currently studying the origin of this discrepancy. Once the simulation accurately describes *both* reflected and transmitted spectra we will be able to produce a detector design with maximum transparency in a selected wavelength range, following the method explained in our previous work [5].
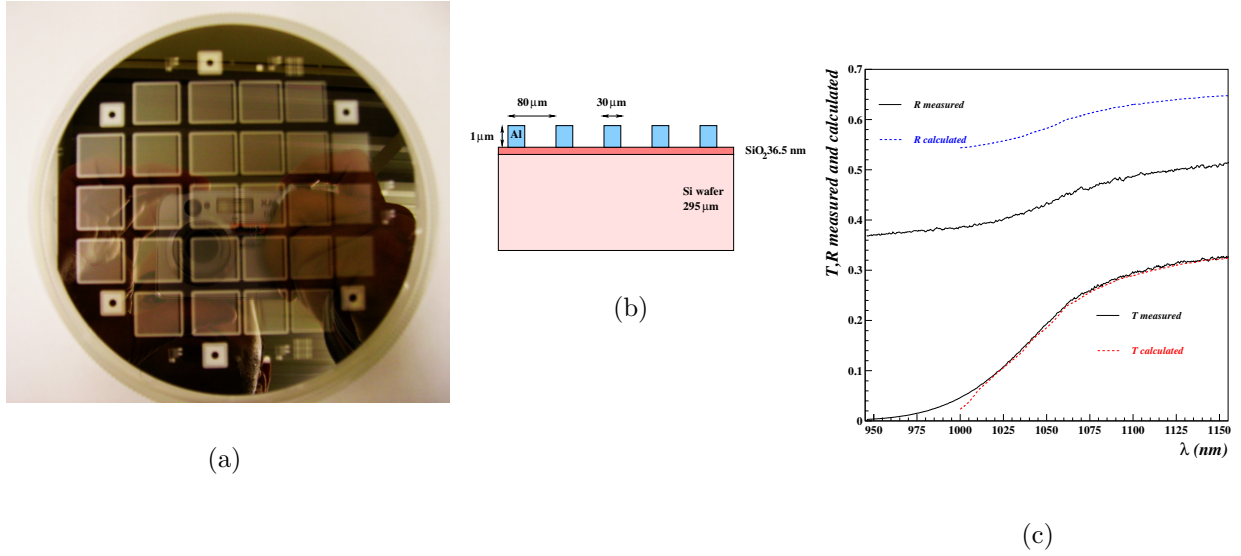
10

Figure 12: a) Wafer with strips b) Sketch of the multilayer grating c) Comparison of measured (black, continuous line) and fit (dashed lines) transmittance (red) and reflectance (blue)

5 Optical measurements of HPK sensors

Besides the R&D line on improvement of microstrip detectors for maximum transmittance in the IR, the other commitment of IFCA within the EUDET project is the implementation of an alignment system for the SiTRA (Silicon Tracking) work package. We modified 5 out of the 30 Hamamatsu sensors [6] to be aligned with lasers. The difference with respect to standard sensors is the absence of Al in a circular spot in the back of the sensor. This Al coating has been etched away after the fabrication process. Differently from the AMS and CMS experiments, the backside of the sensor has not been treated by an antireflection coating (ARC). A picture of a modified alignment sensor is shown in Fig. 13.a. The Al-free spot can be seen in the intersection of the cross-like bands. These bands are not needed for alignment. They will be removed in next versions of the detectors.

Alignment sensors were optically measured before mounting them into modules. Fig. 13.b shows a total of 22 measurements made on 3 sensors across the central spot (1 cm diameter). Superimposed we show a profile histogram which shows the average transmittance with a resolution of 4 nm/bin. Both, mean value and spread coincide well with measurements of CMS sensors produced by HPK with similar layout.

Once mounted, these sensors have been measured using a pulsed 1060 nm laser diode, using the VA1 chips for readout and the DAQ developed by the Paris-LPHNE group [24]. Fig. 13.c shows the gaussian spot of the laser intensity reconstructed by an alignment sensor at 2 different laser positions.
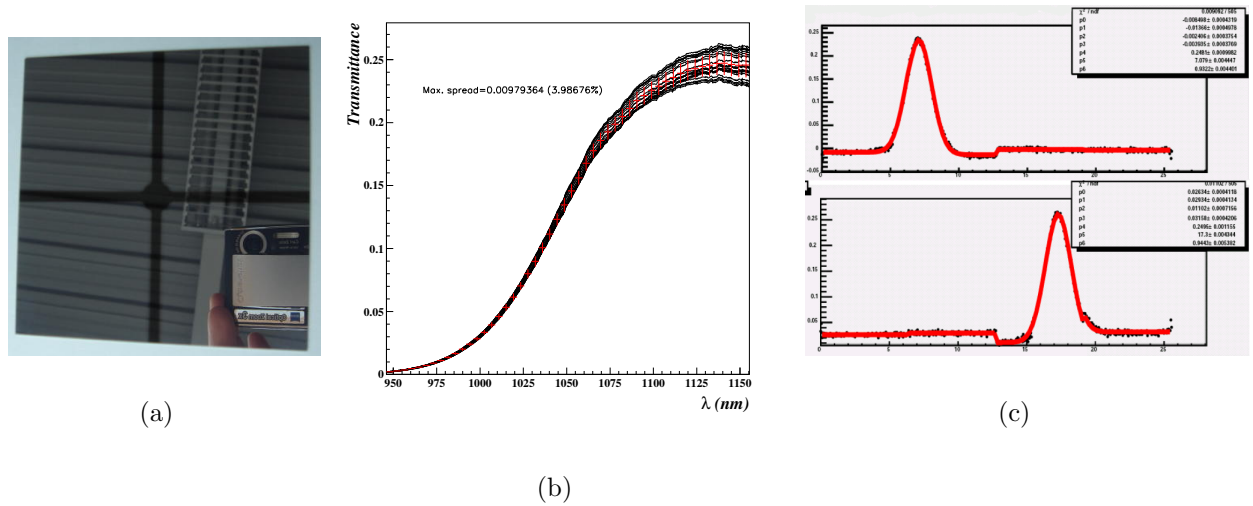
(a)

(b)

(c)

Figure 13: a) Picture of the backside of an alignment friendly sensor. b) Traces correspond to measured transmittance of the central spot of 3 alignment modified sensors. The profile histogram (red bars) has 50 bins. c) Fits of two measured laser spots on one of the alignment modified HPK sensors.

6 Summary and conclusions

The optimization of Silicon microstrip detectors for maximum transmittance needs a full optical simulation of the interferential and diffractional processes inside the detectors. The input to such simulation is the refraction index and thicknesses of each material, and the layout of the strips.

We calculate the refraction index of each layer from samples of materials on Si wafers. The samples are measured and a continuous layer simulation is used to calculate the refraction index for each wavelength. This piece of simulation has been validated reproducing measurements of calibrated layers of SiO_2 on a Si wafer. The thickness of the SiO_2 bands could be predicted with an error of few nm.

We have also presented a novel method to calculate the real part of the refraction index n and the product kd as a function of the wavelength, near the bandgap of Si, using only measurements of the first reflected and transmitted beams. The information obtained is afterwards used as a gaussian constraint in the global fit of T,R for a Silicon slab.

The full optical simulation including diffraction effects has been partially validated. We first compared our calculated T,R with other published simulation results. The agreement with these former works is quite accurate. Comparison to a real diffraction grating produced by CNM has shown a partial agreement only: while the transmittance figure has been perfectly matched, the calculated reflectance is still significantly higher than the measured one. More work on this front is on-going.

Finally we have validated the infrared beam alignment concept proving that a laser signal

can be easily and accurately measured and fitted using a microstrip HPK detector. Three of these alignment modified detectors have been used to integrate the alignment SiTRA prototype.

Acknowledgment

References

[1] W. Wallraff, "TAS status", AMS Tracker Meeting, Montpellier, 22-23 June 2004.

[2] The AMS collaboration, "The Alpha Magnetic Spectrometer (AMS) on the International Space Station, Part I, Results from the test flight on the Space Shuttle", Physics Reports, vol. 366/6 (Aug.2002), pp.331-404.

[3] B. Wittmer et al., "The Laser Alignment System for the CMS Silicon Microstrip Tracker", Nucl. Instr. Meth. A581 (2007)
R. Adolphi, "Construction and Calibration of the Laser Alignment system for the CMS Tracker", PhD Thesis, RWTH-Aachen, Nov. 2006

[4] The CMS collaboration, "CMS Technical Design Report, Volume II: Physics Performance", J. Phys. G, Vol. 34, Num. 6, June 2007

[5] M. Fernández et al., R&D on Microstrip IR Transparent Silicon Sensors, Eudet memo 2007-32
`http://www.eudet.org/e26/e28/e182/e428/eudet-memo-2007-32.pdf`

[6] T.Bergauer, M.Dragicevic, S.Hnsel, M.Krammer et al., Silicon Strip Detector R&D
`http://www.eudet.org/e26/e28/e182/e421/EUDET-MEMO-2007-27.pdf`

[7] Near Infrared Spectrometer, NIR 512L-1.7T1 USB, 523 element InGaAs, single stage TE cooled, Control Development
`http://www.controldevelopment.com`

[8] HL-2000-FHSA-LL, OceanOptics `http://www.oceanoptics.com/ContactUs.asp`

[9] Reflection probe OceanOptics QR400-7-VIS/BX
ControlDevelopment FOC-500-SMA-2M-NIR-fiber optic cable

[10] STAGE-RTL-T, OceanOptics

[11] R.M. Dimeo, "One-Dimensional Convolution and Neutron Spectroscopy", July 11,
2005
`http://www.ncnr.nist.gov/staff/dimeo/idlprograms/convolution.zip`

[12] Max Born and E. Wolf, "Principles of Optics", Second Edition, Pergamon Press

[13] D. L. Windt, "IMD: Software for modeling the optical properties of multilayer
films", Computers in Physics, July 1998, Vol. 12, Issue 4, pp. 360-370

[14] Thin Film reference wafer, OceanOptics

[15] 295± 15 μm TopSiL Si Wafers, `www.topsil.com`

[16] M.J. Keevers, M.A. Green, "Absorption edge of silicon from solar cell spectral
response measurements", Appl.Phys.Lett. 66(2), 174-176, 9 January 1995.

[17] Jon Geist, Silicon (Si) Revisited (1.1-3.1 eV), "Handbook of Optical Constants of
Solids", Academic Press; 1st edition (January 15, 1997)

[18] M.A. Green, M.J. Keevers, "Optical Properties of Intrinsic Silicon at 300 K",
Progress in Photovoltaics: Research and Applicatrions, Vol. 3, 189-192(1995)

[19] D. Delbeke, "Design and fabrication of a highly efficient light-emitting diode: The
grating-Assisted Resonant-Cavity Light-Emitting Diode", INTEC, University of
Ghent, PhD thesis, 2002

[20] B. Dhoedt, D. Delbeke, "RODIS: Rigorous Optical Diffraction Software",
`http://www.photonics.intec.ugent.be/research/facilities/design/rodis/`

[21] K. Knop, J. Opt. Soc. Am., Vol. 68, No. 9, September 1978

[22] M. Auslender, Appl. Optics, Vol 33, No 21, 20 July 1994

[23] Instalación científico tecnológica singular (ICTS): 5ª convocatoria GICSERV de
proyectos de acceso
`http://www.cnm.es/index.php?option=com_content&task=view&id=147&Itemid=233`

[24] High Energy and Nuclear Physics Lab. (LPNHE), IN2P3/CNRS
`http://lpnhe.in2p3.fr/`